

## Supporting Information for

# **Solution-processable, crystalline material for quantitative singlet fission**

Ryan D. Pensack,<sup>a</sup> Christopher Grieco,<sup>b</sup> Geoffrey E. Purdum,<sup>c</sup> Samuel Mazza,<sup>d</sup> Andrew J. Tilley,<sup>e</sup> Evgeny E. Ostroumov,<sup>a</sup> Dwight S. Seferos,<sup>e</sup> Yueh-Lin Loo,<sup>c,f</sup> John B. Asbury,<sup>b</sup> John E. Anthony,<sup>d</sup> and Gregory D. Scholes<sup>a</sup>

<sup>a</sup>Department of Chemistry, Princeton University, Princeton, New Jersey 08544, USA.

<sup>b</sup>Department of Chemistry, The Pennsylvania State University, University Park, Pennsylvania 16802, USA.

<sup>c</sup>Department of Chemical and Biological Engineering, Princeton University, Princeton, New Jersey 08544, USA.

<sup>d</sup>Department of Chemistry, University of Kentucky, Lexington, Kentucky 40506, USA.

<sup>e</sup>Department of Chemistry, University of Toronto, Toronto, Ontario M5S 3H6, Canada.

<sup>f</sup>Andlinger Center for Energy and the Environment, Princeton University, Princeton, New Jersey 08544, USA.

### **Table of Contents:**

- S1. Experimental methods
- S2. Additional details of sample preparation
- S3. Kinetics of the type-I to type-II conversion in the TIPS-pentacene nanoparticles
- S4. The size of the nanoparticles increases slightly with type-I to type-II conversion
- S5. No conversion using either silicone oil or polydimethylsiloxanes as additives
- S6. An alternative means of initiating type-I to type-II conversion
- S7. Type-I TIPS-pentacene nanoparticles are amorphous and type-II TIPS-pentacene nanoparticles are crystalline
- S8. Comparison of transient absorption spectrum obtained at 1 ns from crystalline nanoparticles and film
- S9. Transient near-infrared absorption rules out singlet exciton traps and confirms singlet fission as the primary decay pathway in crystalline TIPS-pentacene nanoparticles

- S10. Global analysis of transient visible absorption of crystalline TIPS-pentacene nanoparticles according to a model including two triplet pair intermediates
- S11. Kinetic-based estimate of singlet-to-triplet conversion efficiency for initial step of singlet fission in crystalline nanoparticles
- S12. Crystalline TIPS-pentacene nanoparticles are insensitive to singlet-singlet annihilation, but highly susceptible to triplet-triplet annihilation
- S13. Comparison of TIPS-pentacene isolated-molecule singlet and triplet excitation spectra with amorphous nanoparticle early- and long-time transient absorption spectra
- S14. Kinetic-based estimate of singlet-to-triplet conversion efficiency for initial step of singlet fission in amorphous nanoparticles
- S15. Alternative, parallel decay pathways such as charge carrier formation and photodimerization are ruled out in the amorphous TIPS-pentacene nanoparticles
- S16. Five-component global and target analysis of the transient visible absorption of the amorphous TIPS-pentacene nanoparticles
- S17. Identical losses are observed in amorphous TIPS-pentacene films
- S18. Singlet and triplet excitations in amorphous TIPS-pentacene nanoparticles are not susceptible to bimolecular annihilation
- S19. Parameters varied to prepare samples of mixed morphologies
- S20. Assignment to mixed-phase nanoparticles over a mixture of pure-phase amorphous and crystalline nanoparticles
- S21. Extinction spectra of crystalline and amorphous TIPS-pentacene nanoparticles
- S22. Migration of excitation energy between nanoparticles is not possible on the timescale of the femtosecond transient absorption measurements
- S23. Films with mixed morphology also do not show evidence for parent singlet exciton migration between amorphous and crystalline domains
- S23. Transient near-infrared absorption of neat and mixed-phase TIPS-pentacene nanoparticles
- S25. Pump pulse autocorrelation
- S26. Supplementary methods
- S27. References

## **Section S1: Experimental methods**

### **Pentacene derivatives**

HPLC-grade ( $\geq 99\%$ ) TIPS-Pn was purchased from Sigma-Aldrich and used as received.

### **Nanoparticle preparation**

To prepare amorphous nanoparticles, 200  $\mu\text{L}$  of an 800  $\mu\text{M}$  solution of TIPS-Pn in reagent-grade tetrahydrofuran (THF; EMD Millipore, Billerica, Maryland) was rapidly injected into a 20 mL glass scintillation vial containing 10 mL of vigorously stirring distilled water. A 21 gauge disposable needle (BD, Franklin Lakes, New Jersey) and 1 mL disposable syringe (Henke-Sass Wolf, Tuttlingen, Germany) were used to inject the TIPS-Pn/THF solution. To crystallize the amorphous nanoparticles, a different procedure was developed as is described in detail in **Section S2**. Briefly, 500  $\mu\text{L}$  of an 320  $\mu\text{M}$  solution of TIPS-Pn in reagent-grade THF (EMD Millipore, Billerica, Maryland) cooled to a temperature of 5  $^{\circ}\text{C}$  was drawn into a 1 mL disposable syringe (BD, Franklin Lakes, New Jersey) and agitated within the barrel at least five times. The TIPS-Pn/THF solution was then rapidly injected into a 20 mL glass scintillation vial containing 10 mL of vigorously stirring distilled water. The resulting aqueous colloidal TIPS-Pn nanoparticle suspension was subsequently transferred to another vial and stored in a refrigerator at a temperature of 5  $^{\circ}\text{C}$ . For transient absorption measurements, the nanoparticle suspensions were concentrated by combining four 10 mL batches together and subjecting the total solution to rotary evaporation at 18 mbar and 35  $^{\circ}\text{C}$  for a period of ca. 40-50 min.

### **Film preparation**

Amorphous films of TIPS-Pn were prepared in a manner described previously.<sup>1</sup> All films were made by spin-coating 20 mg/mL dichloromethane solutions onto sapphire substrates at  $\sim 1600$  rpm. The amorphous films were crystallized by solvent-vapor annealing for 2.5 hr with isopropyl alcohol using an annealing apparatus described in detail previously.<sup>1</sup> For preparing films having mixed morphology of both amorphous and crystalline domains, the amorphous films were solvent-vapor annealed similarly, except for shorter amounts of time ranging from 5-6 min.

### **Steady-state absorption spectroscopy**

Absorption spectra were measured using either an Agilent Cary 60 spectrophotometer (Agilent Technologies, Santa Clara, CA) or an Agilent Cary 6000i UV-vis-NIR spectrophotometer (Agilent Technologies, Santa Clara, CA) equipped with an integrating sphere detector.

### **Femtosecond transient absorption spectroscopy**

Femtosecond transient absorption measurements were performed with a spectrometer that has been described in detail previously.<sup>2</sup> In brief, measurements were performed with a 1 kHz regeneratively amplified Ti:sapphire laser system (Coherent Libra, Santa Clara, California) that delivers  $\sim 45$  fs pulses at  $\sim 800$  nm with an average power of  $\sim 4$  W. A beamsplitter situated at the output of the laser amplifier served to generate pump and probe beam paths. A large fraction of the power was

used in the pump beam path to drive an optical parametric amplifier (Light Conversion OPerA, Vilnius, Lithuania) and convert the 800 nm light to wavelengths in the range of 645-700 nm, that are reported as appropriate in the main text. The pump and a small fraction of the direct laser amplifier output were guided into a commercial transient absorption spectrometer (Ultrafast Systems Helios, Sarasota, Florida). The latter was used to generate a continuum in either the visible (ca. 420 to 760 nm) or near-infrared (ca. 850 to 1600 nm) spectral region. Excessive amounts of 800 nm radiation overlapping the continuum were reduced through the use of appropriately selected optical filters. Before the continuum generation crystal, a combination of a  $\lambda/2$  waveplate and polarizer in the probe beam path were used to control the relative pump and probe polarization. Measurements were performed with the magic angle at the sample. The nanoparticle suspensions were contained in a 2 mm path length glass spectrophotometer cell (Starna Cells, Inc., Atascadero, California) and were stirred over the course of the measurement with a magnetic stir bar situated within the sample cell driven by a rotating magnetic metal rod. The sample optical densities ranged between ca. 0.2 and 0.35 at the pump wavelength. The pump beam spot size was determined by placing a digital CCD camera (Thorlabs Inc., Newton, New Jersey) at focal plane of the probe in the region of pump and probe overlap and analyzing an image obtained using ThorCam software (Thorlabs Inc., Newton, New Jersey). The spot size determined in this manner was ca. 180 and 160  $\mu\text{m}$  for ca. 645 and 700 nm pump wavelengths, respectively. An optical power sensor and meter (Coherent Inc., Santa Clara, California) was used to measure pulse energies. The incident pump fluences for the different measurements are reported where appropriate. The pump pulse duration at a wavelength of 710 nm, measured by performing an autocorrelation measurement, was determined to be ca.  $110 \pm 5$  fs (**Section S25**).

## **Section S2: Additional details of sample preparation**

In order to achieve complete type-I to type-II conversion and to ensure reproducibility, we found it necessary to modify our published procedure<sup>3</sup> in the following manner: (i) a disposable syringe including a silicone-based lubricant was used, (ii) the TIPS-Pn / THF solution was drawn into the barrel of the syringe and agitated several times (a crude means of quantifying the agitation is illustrated in **Figure S1**), (iii) the volume of the TIPS-Pn / THF solution injected was increased and its concentration was reduced, (iv) the TIPS-Pn / THF solution was maintained at a lower temperature prior to injection, and (v) the aqueous colloidal nanoparticle suspension was stored at a lower temperature immediately following its preparation. With regard to (iv) and (v), we found 5 °C to be an optimal injection and storage temperature.

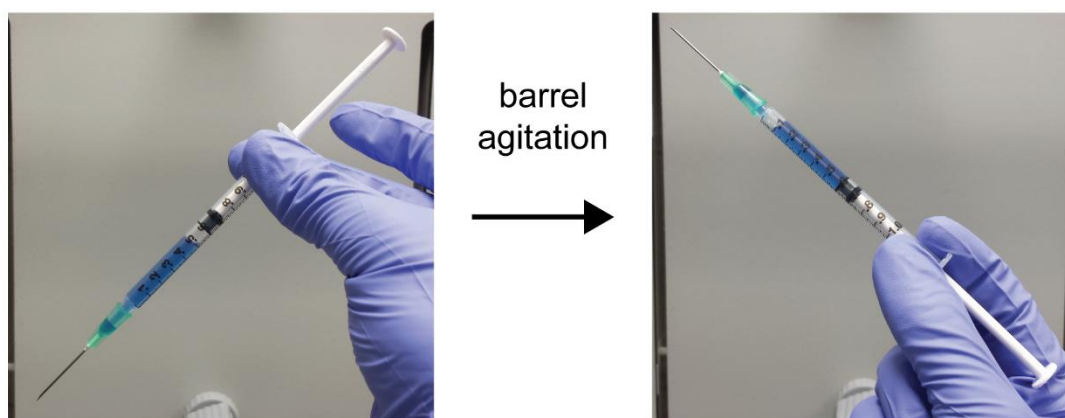


**Figure S1.** An illustration of the most reproducible way in which to introduce additive into the pentacene derivative / THF solution by agitating the solution within the barrel of a syringe containing a silicone-based lubricant. The syringe was essentially flipped so as to make contact with the black, elastomeric stopper, and then returned to its starting position.

A detailed description of the experimental conditions necessary to achieve complete and reproducible type-I to type-II conversion are listed below.

Volume of water: 9.5 mL

Water temperature: 21 °C

TIPS-pentacene / THF solution concentration: 320  $\mu$ M

TIPS-pentacene / THF solution volume: 500  $\mu$ L

TIPS-pentacene / THF solution temperature: 5 °C

Syringe: BD 1mL Luer-Lok™ Syringe (BD, Franklin Lakes, New Jersey)

Number of times agitated within barrel (prior to injection): 5

Suspension storage temperature: 5 °C

### Section S3: Kinetics of the type-I to type-II conversion in the TIPS-pentacene nanoparticles

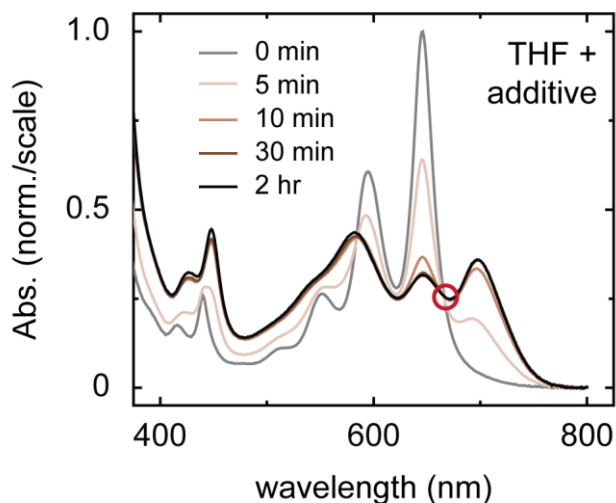


**Figure S2.** Absorption spectra of TIPS-pentacene nanoparticles measured as a function of time following injection of the TIPS-pentacene / THF solution. The “0 min” spectrum was technically obtained ca. 30-90 seconds following injection; this was the time it took to transfer the solution to the cuvette, and perform the measurement. The other measurements were obtained in the same manner, but after storing samples for the specified period of time in a refrigerator held at 5 °C. The spectra have essentially converged after ca. 30 min. Note that because the nanoparticle suspensions were prepared independently, the absorbance of the 2 hr spectrum did not match that of the other four spectra in the vicinity of the isosbestic point at ca. 665 nm (highlighted by the red circle in the plot) owing to batch-to-batch variation that resulted in a slightly different nanoparticle concentration. To account for this slight difference in concentration, the 2 hr spectrum was scaled by a factor of 1.05 such that its amplitude was made to match the amplitude of the other spectra in the region of the isosbestic point.

**Section S4: The size of the nanoparticles increases slightly with type-I to type-II conversion**

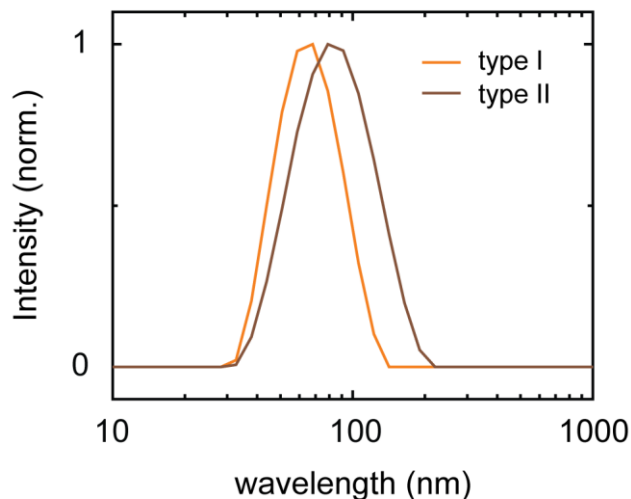


**Figure S3.** Results of dynamic light scattering measurements on the neat type-I and type-II TIPS-pentacene nanoparticles.

Using dynamic light scattering, we measured a diameter of ca. 70 and 80 nm for the neat type-I and type-II TIPS-pentacene nanoparticles, respectively (**Figure S3**). Owing to potential batch-to-batch variation, as might result from Ostwald ripening for samples with different storage times,<sup>4</sup> we have refrained from drawing any specific conclusions from these results. We can, however, use the results to draw two very general conclusions: (i) the diameter of the nanoparticles is generally of the order of ca. 100 nm or less, and (ii) the size of the nanoparticles is not significantly altered over the course of the type-I to type-II conversion.

**Section S5: No conversion using either silicone oil or polydimethylsiloxanes as additives**

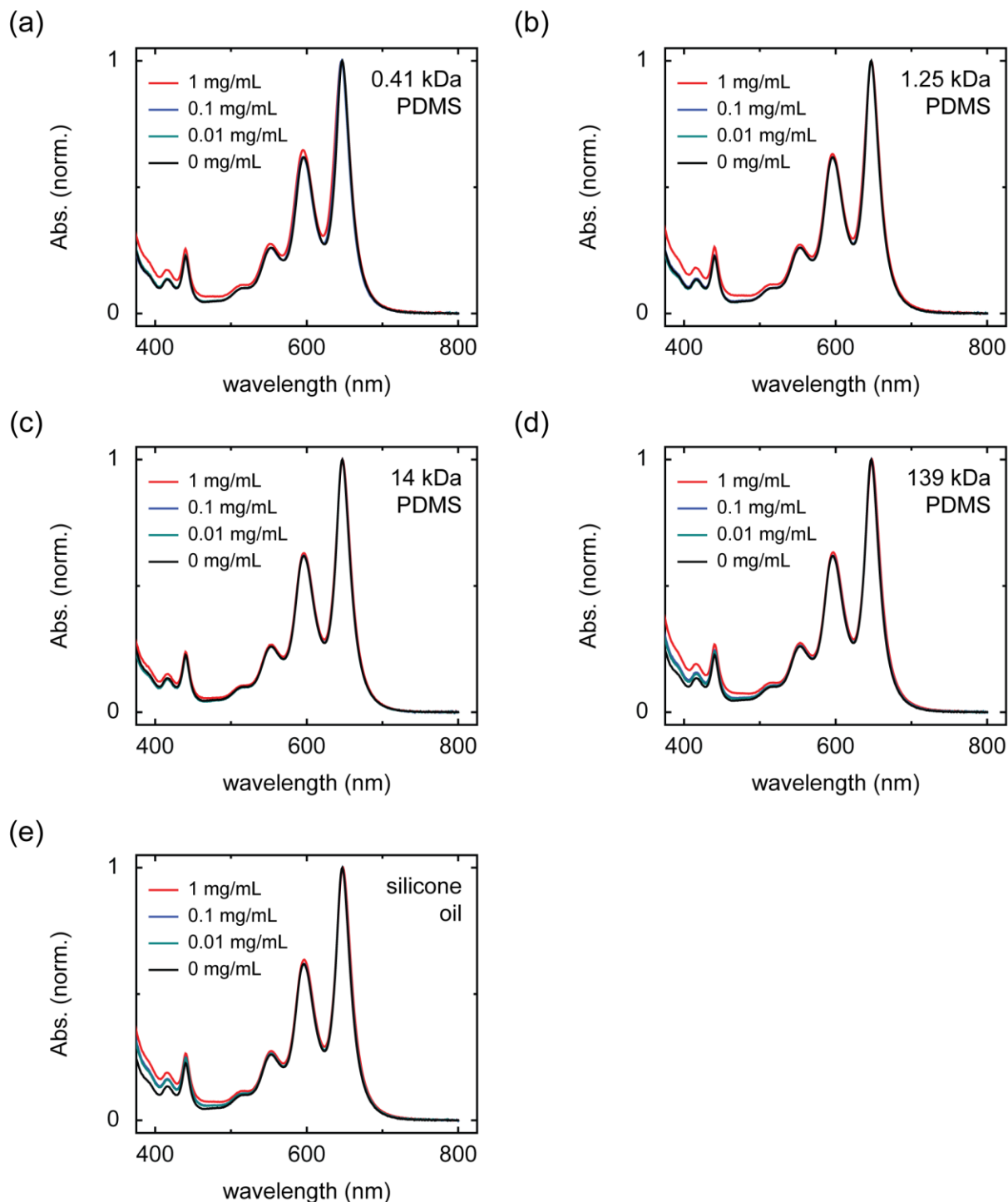


**Figure S4.** Absorption spectra of nanoparticles prepared using a syringe lacking a silicone-based lubricant, but including in the TIPS-pentacene/THF injection solution various concentrations of the additives (a) 0.41 kDa polydimethylsiloxanes, (b) 1.25 kDa polydimethylsiloxanes, (c) 14 kDa polydimethylsiloxanes, (d) 139 kDa polydimethylsiloxanes, and (e) silicone oil.

## **Section S6: An alternative means of initiating type-I to type-II conversion**

Over the course of developing our method (and over the course of attempting to track down the chemical origin of the type-I to type-II conversion), we identified another way to initiate type-I to type-II conversion in the TIPS-pentacene nanoparticles. The alternative approach involves injecting the concentrated TIPS-pentacene / THF solution into a solution of polyvinyl alcohol in water. We found the polyvinyl alcohol / water solution concentration to sensitively influence the extent of the type-I to type-II conversion (**Figure S5**).

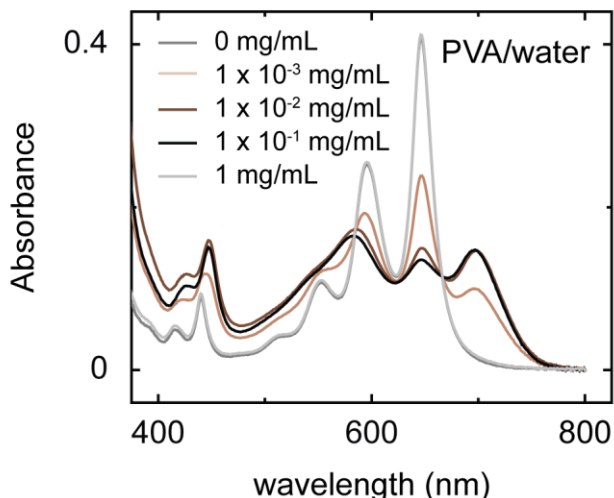


**Figure S5.** Absorption spectra of TIPS-pentacene nanoparticles prepared by injecting the TIPS-pentacene / THF solution into a rapidly stirring solution of polyvinyl alcohol in water. The spectra were obtained 30 minutes following injection. Note that because the nanoparticle suspensions were prepared independently, the absorbance of the entire set of spectra did not match in the vicinity of the isosbestic point at ca. 665 nm owing to batch-to-batch variation that resulted in a slightly different nanoparticle concentration. To account for this slight difference in concentration, the spectra of the 0 mg/mL and  $1 \times 10^{-1}$  mg/mL were scaled by a factor of 1.05 and 0.95, respectively, such that their amplitude was made to match the amplitude of the other spectra in the region of the isosbestic point (determined according to where the spectra of the  $1 \times 10^{-3}$  mg/mL,  $1 \times 10^{-2}$  mg/mL, and 1 mg/mL samples overlapped).

Clearly type-I to type-II conversion is possible according to this approach, and furthermore we find that the extent of the type-I to type-II conversion depends sensitively on the concentration of the polyvinyl alcohol / water solution.

## Section S7: Type-I TIPS-pentacene nanoparticles are amorphous and type-II TIPS-pentacene nanoparticles are crystalline

In the main text, we compared the type-I and type-II nanoparticle absorption spectra with that of amorphous and crystalline films (Figs. 1b and 1c). “As-cast” films were deposited from a 10 mg/mL solution in chloroform via spin-coating at 2000 rpm. The films were subsequently crystallized by solvent-vapor annealing with toluene as the vapor source. We performed two-dimensional grazing-incidence X-ray scattering (2D GIWAXS) measurements to verify the solid-state order of the films (Figure S6).

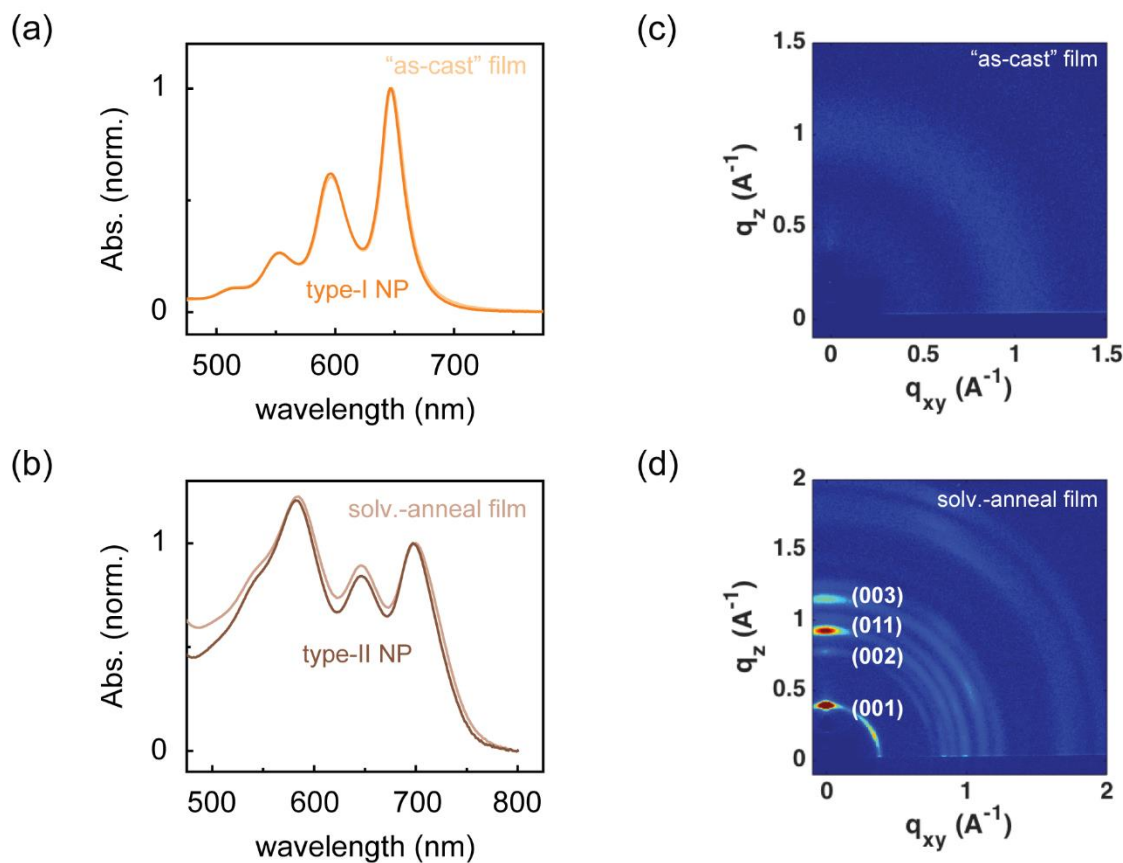


**Figure S6.** (a,b) Steady-state absorption spectra of TIPS-pentacene processed into aqueous type-I and type-II nanoparticle suspensions and “as-cast” and solvent-vapor annealed films. The absorption spectra have been normalized to the peak of the lowest-energy singlet absorption. (c,d) Two-dimensional grazing-incidence X-ray diffraction patterns of “as-cast” and solvent-vapor annealed films of TIPS-pentacene. The peaks in the X-ray diffraction pattern were indexed according to the known equilibrium structure of TIPS-pentacene (CCDC # 172476).

For convenience, we have replotted the absorption spectra from the main text as panels a and b in Figure S6. The 2D GIWAXS patterns corresponding to the films are shown in panels c and d, and confirm that the films are amorphous and crystalline.

**Section S8: Comparison of transient absorption spectrum obtained at 1 ns from crystalline nanoparticles and film**

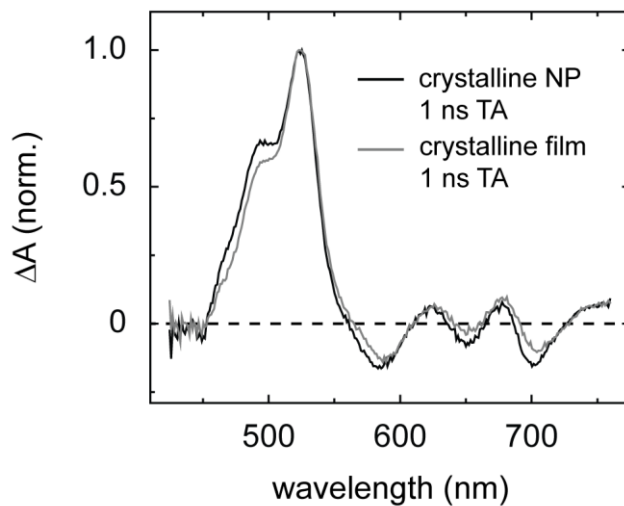


**Figure S7.** Transient absorption spectrum obtained at 1 ns from crystalline nanoparticles and film. The pump wavelength for both measurements was 700 nm, and the incident pump fluence for the measurements on the crystalline nanoparticles and film were 5 and 10  $\mu\text{J}/\text{cm}^2$ , respectively.

**Section S9: Transient near-infrared absorption rules out singlet exciton traps and confirms singlet fission as the primary decay pathway in crystalline TIPS-pentacene nanoparticles**

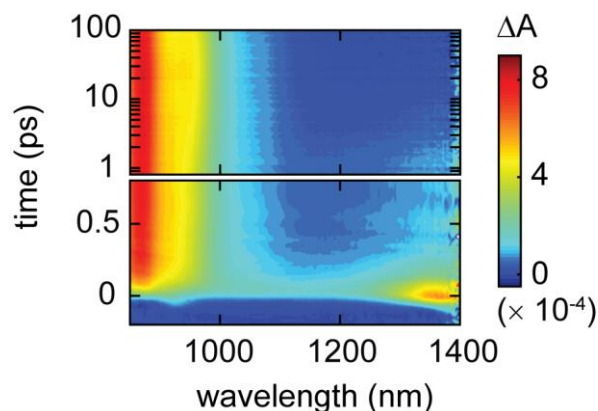
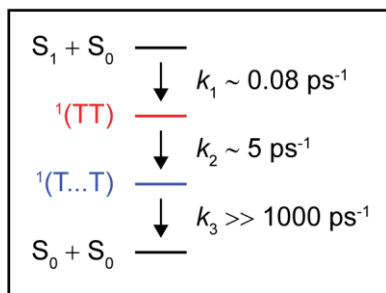


**Figure S8.** Surface plot of transient near-infrared absorption spectra of crystalline TIPS-Pn nanoparticles. The experiments were performed with an incident pump fluence of ca.  $65 \mu\text{J}/\text{cm}^2$ . A reference dataset on just the solvent was subtracted from these data to suppress signals arising from the nonresonant response of the medium. Two photoinduced absorption bands associated with parent singlet and triplet populations appear in this spectral region: (i) the parent singlet photoinduced absorption which has a strong origin band at ca. 1400 nm, and (ii) the triplet photoinduced absorption which has a weak origin band at ca. 1080 nm, and becomes progressively more intense at shorter wavelengths.

**Section S10: Global analysis of transient visible absorption of crystalline TIPS-pentacene nanoparticles according to a model including two triplet pair intermediates**

(a)

kinetic scheme:



(b)

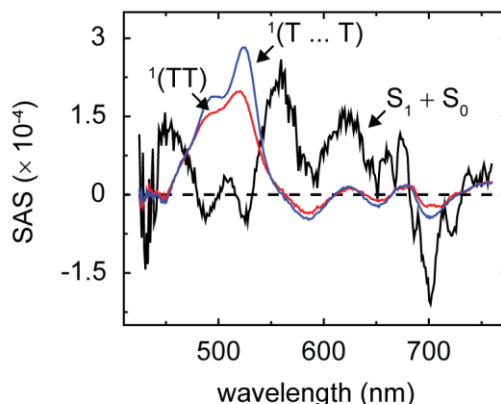


**Figure S9.** Global analysis of transient visible absorption of crystalline TIPS-pentacene nanoparticles. (a) Three-component kinetic scheme used to model the transient visible absorption of the crystalline TIPS-pentacene nanoparticles. The experiments were performed with an incident pump fluence of  $5 \mu\text{J}/\text{cm}^2$ ; the data that was modeled is reported in the main text (**Figure 2a**). The time constants resulting from the analysis are indicated. (b) Species-associated spectra resulting from a three-component analysis of the transient absorption data. The first component (black) is associated with parent singlet excitons. The second and third components (red and blue) are associated with nascent and spatially separated triplet pair intermediates, respectively.

### **Section S11: Kinetic-based estimate of singlet-to-triplet conversion efficiency for initial step of singlet fission in crystalline nanoparticles**

We can make a simple kinetic argument,<sup>5</sup> as has been done historically,<sup>6</sup> to estimate the efficiency of the initial singlet-to-triplet conversion. In brief, the idea is to use the rate of the initial step of singlet fission and that of all other processes to make this estimation. The rate of decay of the isolated molecule in solution serves as a useful estimate of the latter. For TIPS-pentacene in toluene, this value is ca. 12 ns.<sup>7</sup> According to this estimate, we find that 99.999%, or effectively 100%, of the parent singlet excitons are converted to triplet pairs in crystalline TIPS-Pn; an estimate in line with the general understanding.<sup>3,8,9</sup>

For example, taking the rate of triplet pair formation,  $k_{1(TT)}$ , in the crystalline nanoparticles as

$$k_{1(TT)} \approx (1/0.1) \text{ ps}^{-1}$$

And the rate of all other competing processes,  $k_{\text{other}}$ , as

$$k_{\text{other}} \approx k_{\text{F}} = (1/12) \text{ ns}^{-1}$$

We estimate the quantum yield for triplet pair formation,  $\Phi_{1(TT)}$ , in the crystalline nanoparticles to be

$$\Phi_{1(TT)} \approx k_{1(TT)} / [k_{1(TT)} + k_{\text{other}}] = 99.999\%$$

**Section S12: Crystalline TIPS-pentacene nanoparticles are insensitive to singlet-singlet annihilation, but highly susceptible to triplet-triplet annihilation**

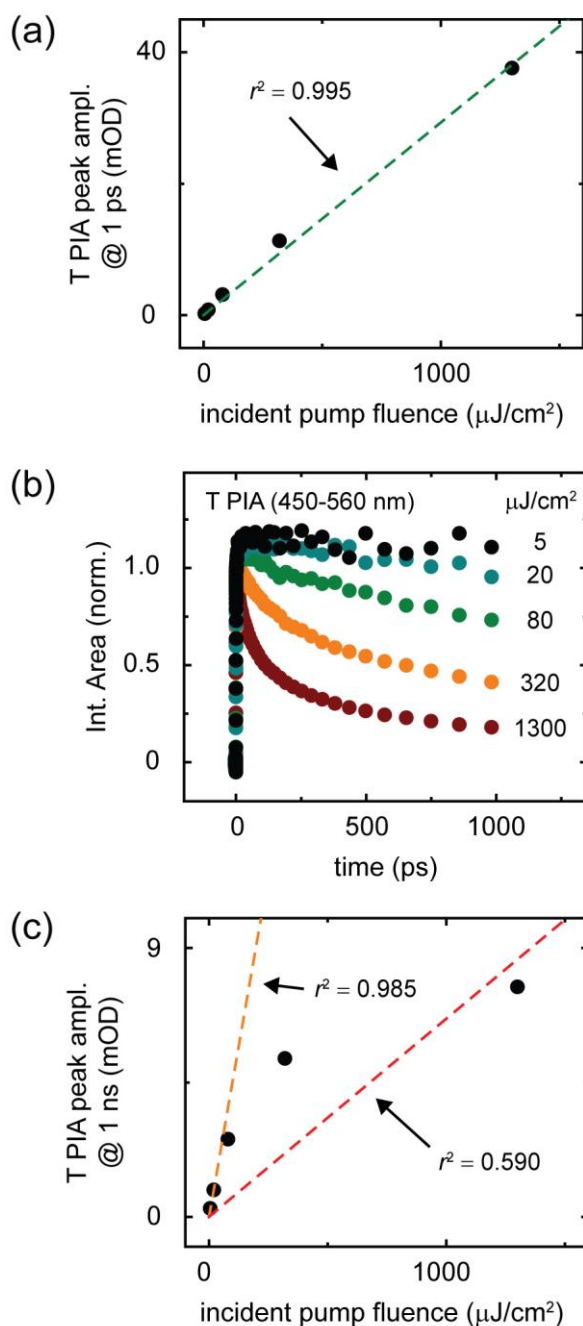


**Figure S10.** Fluence-dependent transient absorption measurements of crystalline TIPS-pentacene nanoparticles. (a) Peak amplitude in the vicinity of the origin band of the triplet photoinduced absorption in the visible spectral region (i.e., ca. 523 nm) at a time delay of ca. 1 ps plotted as a function of incident pump fluence. Overlaying the data is a linear fit (green dashed line) with  $r^2 = 0.995$ . (b) Integrated area of the triplet photoinduced absorption band in the visible spectral region (i.e., ca. 450-560 nm) plotted at several incident pump fluences as a function of time delay. The

data were normalized to the integrated area at a time delay of ca. 1 ps. (c) Peak amplitude in the vicinity of the origin band of the triplet photoinduced absorption in the visible spectral region (i.e., ca. 525 nm) at a time delay of ca. 1 ns plotted as a function of incident pump fluence. Overlaying the data is a linear fit to the first two data points (orange dashed line), with  $r^2 = 0.985$ . A linear fit including all five data points (red dashed line) gave  $r^2 = 0.590$ . An  $r^2$  value deviating from unity by more than 1% was taken as an indicator of nonlinearity.

While the singlet exciton population in the crystalline TIPS-Pn nanoparticles is not susceptible to bimolecular annihilation (**Figure S10a**), we found the triplet excitation population in the crystalline TIPS-Pn nanoparticles to be highly susceptible to bimolecular annihilation (**Figures S10b and S10c**). Specifically, we found the peak amplitude in the vicinity of the origin band of the triplet photoinduced absorption in the visible spectral region (i.e., at ca. 523 nm) at a time delay of ca. 1 ps, i.e., that associated with the triplet pair population directly populated by parent singlet excitons, to show excellent linearity even at incident pump fluences as high as 1.3 mJ/cm<sup>2</sup> (**Figure S10a**). Thus, as a consequence of the exceedingly fast decay of the parent singlet population into triplet pairs (i.e., on a sub-100-fs timescale) in crystalline TIPS-Pn, any potential bimolecular singlet-singlet annihilation at early timescales is negligible even at exceedingly high incident pump fluences. The triplet exciton population in the crystalline TIPS-Pn nanoparticles, in contrast, undergoes substantial bimolecular annihilation on pico- and nanosecond timescales (**Figure S10b**). The data in **Figure S10b** plot the kinetics of the integrated area of the triplet photoinduced absorption band in the visible spectral region (i.e., ca. 450-560 nm) at several incident pump fluences. The data were normalized to the integrated area at a time delay of 1 ps, which as we showed in **Figure S10a** is essentially linear with incident pump fluence. The pronounced triplet-triplet annihilation observed in the crystalline TIPS-Pn nanoparticles is especially apparent when comparing **Figures S10a and S10c**, the latter of which plots the peak amplitude in the vicinity of the origin band of the triplet photoinduced absorption in the visible spectral region (i.e., ca. 525 nm) at a time delay of ca. 1 ns, i.e., a timescale several orders-of-magnitude larger than that associated with triplet transfer in crystalline material (see e.g. **Section S10** where we derive a triplet transfer time constant of ca. 5 ps). While the data presented in **Figure 10a** are essentially linear at all incident pump fluences, the data presented in **Figure 10c** show obvious (and substantial) deviations from linearity.

We conclude that there is no singlet-singlet annihilation in the crystalline TIPS-Pn nanoparticles even at exceptionally high incident pump fluences, further highlighting the effectiveness and efficiency of singlet fission as a decay pathway for parent singlet excitons (c.f. **Section S11**). The triplet excitation population in the crystalline TIPS-Pn nanoparticles, in contrast, is highly sensitive to incident pump fluence as is evident by substantial bimolecular annihilation on the pico- and nanosecond timescales.

**Section S13: Comparison of TIPS-pentacene isolated-molecule singlet and triplet excitation spectra with amorphous nanoparticle early- and long-time transient absorption spectra**

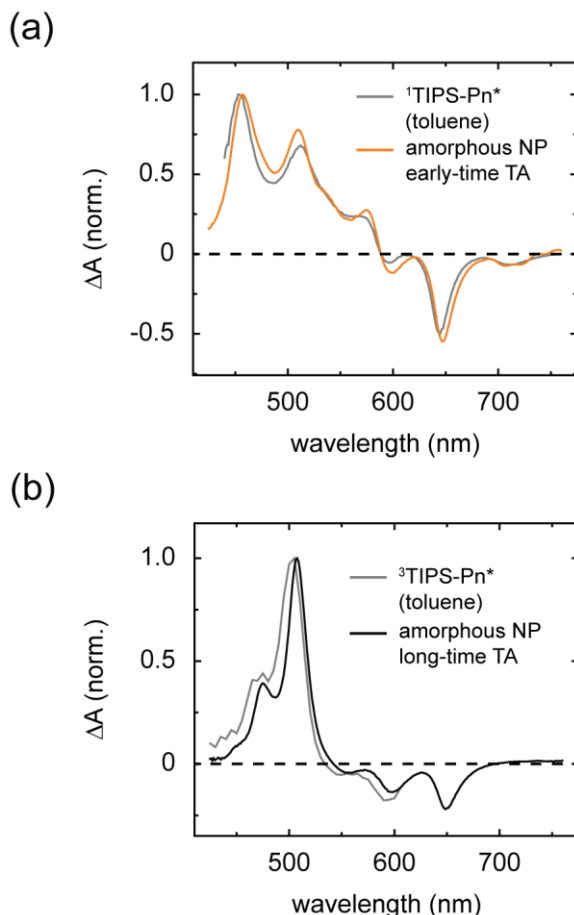


**Figure S11.** (a) Comparison of isolated-molecule singlet excitation spectrum with early-time transient absorption spectrum of amorphous nanoparticles. The measurements were obtained with an incident pump wavelength of 645 nm and incident pump fluences of ca. 240 and 60  $\mu\text{J}/\text{cm}^2$ , respectively. The isolated-molecule singlet excitation spectrum was obtained by time-averaging the transient absorption of a dilute solution of TIPS-pentacene in toluene over the range 1 to 1000 ps whereas the early-time transient absorption spectrum of the amorphous TIPS-pentacene nanoparticles was obtained at a time delay of ca. 0 ps in the vicinity of the pulse overlap. The isolated-molecule singlet excitation spectrum and early-time amorphous nanoparticle transient absorption spectrum are very similar, consistent with an interpretation that the population at early time in the amorphous nanoparticles is primarily parent singlet excitations. (b) Comparison of isolated-molecule triplet excitation spectrum with long-time transient absorption of amorphous nanoparticles. The experiments were performed with incident pump wavelengths of 642 and 645 nm and incident pump fluences of ca. 200 and 60  $\mu\text{J}/\text{cm}^2$ , respectively. The isolated-molecule triplet excitation spectrum was obtained by time-averaging the transient absorption of a dilute solution of TIPS-pentacene in toluene over the range 200 to 1000 ns whereas the long-time transient absorption spectrum of the amorphous TIPS-pentacene nanoparticles was obtained at a time delay of ca. 1 ns. The isolated-molecule triplet excitation spectrum and long-time amorphous

nanoparticle transient absorption spectrum are very similar, consistent with the interpretation that parent singlet excitations have been converted into triplet pair excitations via singlet fission in the amorphous nanoparticles.

### **Section S14: Kinetic-based estimate of singlet-to-triplet conversion efficiency for initial step of singlet fission in amorphous nanoparticles**

We take the same approach as in **Section S11** above to estimate the singlet-to-triplet conversion efficiency for the initial fission in the amorphous TIPS-pentacene nanoparticles. In this case, the initial rate of triplet pair formation is slightly slower. The influence of the slower rate on the overall singlet-to-triplet conversion is outlined below:

Again, taking the rate of triplet pair formation,  $k_{1(\text{TT})}$ , in the amorphous nanoparticles as

$$k_{1(\text{TT})} \approx (1/1.2) \text{ ps}^{-1}$$

And the rate of all other competing processes,  $k_{\text{other}}$ , as

$$k_{\text{other}} \approx k_{\text{F}} = (1/12) \text{ ns}^{-1}$$

We estimate the quantum yield for triplet pair formation,  $\Phi_{1(\text{TT})}$ , in the amorphous nanoparticles to be

$$\Phi_{1(\text{TT})} \approx k_{1(\text{TT})} / [k_{1(\text{TT})} + k_{\text{other}}] = 99.99\%$$

## Section S15: Alternative, parallel decay pathways such as charge carrier formation and photodimerization are ruled out in the amorphous TIPS-pentacene nanoparticles

We carefully considered the possibility that alternative, parallel decay pathways such as charge carrier formation and photodimerization could contribute appreciably to the excited-state dynamics in the amorphous TIPS-Pn nanoparticles.

We first considered charge carrier formation as a possible alternative decay pathway. To test whether or not features in the transient absorption spectra are assignable to charge carriers, we compared the intermediate-time delay spectrum measured for the amorphous TIPS-Pn nanoparticles (i.e., at a time delay of 20 ps) with the absorption spectra of TIPS-Pn anions and cations (**Figure S12**).

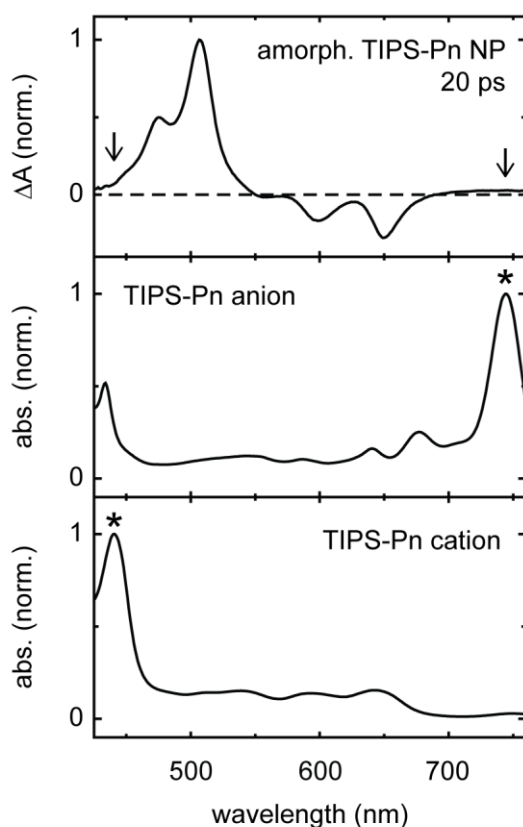


**Figure S12.** The figure above displays the intermediate time-delay (20 ps) transient absorption spectrum observed in amorphous TIPS-Pn nanoparticles (upper panel), the spectrum of TIPS-Pn anions generated via chemical reduction using sodium metal (middle panel), and the spectrum of TIPS-Pn cations generated electrochemically through cyclic voltammetry (bottom panel). Strong bands associated with the anion and cation are highlighted by asterisks, and arrows point to where these bands should be evident in the intermediate time-delay transient absorption spectrum of the amorphous TIPS-Pn nanoparticles.

TIPS-Pn cations have a strong absorption feature peaking at ca. 440 nm, and anions have a strong absorption feature peaking at ca. 745 nm (each highlighted by an asterisk in the plot). Arrows are placed in the plot of the intermediate-time delay transient absorption spectrum where the sharp bands corresponding to the cation and anion would appear if charge carriers are formed. Clearly, the intermediate-time delay transient absorption spectrum does not show any evidence of these induced absorption bands. These observations are consistent with the basic physics of organic semiconductors,<sup>10</sup> namely that they are low dielectric constant materials that exhibit localized carrier wavefunctions,<sup>11</sup> and the general expectation that charge carriers are unlikely to form in the amorphous TIPS-Pn nanoparticles under the conditions in which the present measurements were performed. Therefore, we conclude that charge carriers are not formed in an appreciable yield in the amorphous TIPS-Pn nanoparticles.

We next considered photodimerization as a possible alternative decay pathway. The formation of photodimers, which are known to be permanent photoproducts in pentacene and its derivatives, would give rise to a permanent bleach feature in the transient absorption measurement. **Figure S13a** shows a transient absorption spectrum of the amorphous TIPS-Pn nanoparticles obtained at a long time delay of ca. 1 ms (limited by the repetition rate of the laser light source of 1 kHz).

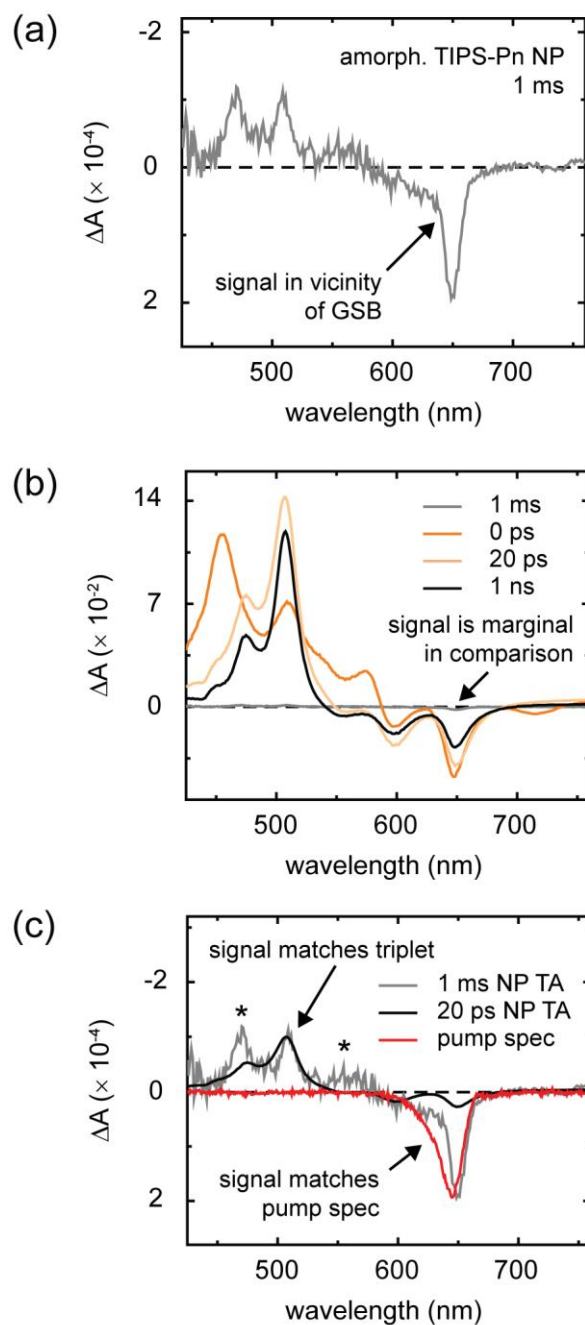


**Figure S13.** (a) Transient absorption spectrum of amorphous TIPS-Pn nanoparticles obtained at a time delay of 1 ms. No background subtraction was performed on these data. (b) Transient absorption spectra of the amorphous TIPS-Pn nanoparticles obtained at time delays as reported in the main text of the manuscript, but without any background subtraction. (c) 1 ms transient absorption spectrum overlaying a scaled and inverted spectrum of the pump pulse along with a scaled transient absorption spectrum of triplet pairs (i.e., 20 ps). Signals in the 1 ms transient absorption spectrum that cannot be explained by either pump scatter or long-lived triplet excitations are highlighted with an asterisk.

In the 1 ms transient absorption spectrum, we observe signal in the vicinity of the ground state bleach. **Figure S13b** shows that this signal is marginal in comparison with that observed at much shorter time delay. Specifically, taking the ratio of the area of the 1 ms and 0 ps transient spectra integrated over the range from 630 to 690 nm, we obtain a value of 3%. Thus, the signal observed at exceedingly long time delay, which could have a contribution from a parallel decay pathway such as photodimerization, represents at most 3% of the signal observed at the time origin of the measurement. If this signal were entirely attributable to photodimerization, and operating within the framework of a strict definition of the term “quantitative”, we would need to reconsider our interpretation that the first step of singlet fission, i.e., triplet pair formation, is quantitative in the amorphous TIPS-Pn nanoparticles because such a loss would correspond to a triplet pair formation efficiency of ca. 97% (i.e., less than 100%).

**Figure S13c** shows that the evidence for this signal as entirely arising from photodimerization is weak. In **Figure 13c**, we compare the 1 ms transient spectrum with an inverted and scaled spectrum of the pump pulse.<sup>12</sup> Clearly, there is good agreement with the pump spectrum and the signal in the vicinity of the ground-state bleach feature. Thus, the signal in the vicinity of the ground-state bleach feature likely has a large contribution from pump scatter, as would be expected from a nanoparticle suspension, and this contribution would serve to decrease the value of the upper limit we established above of 3% for photodimerization. In **Figure 13c**, we also compare the 1 ms transient spectrum to the triplet pair spectrum (i.e., the 20 ps transient absorption spectrum), scaled such that its induced absorption peak at ca. 510 nm matches that of the 1 ms transient spectrum. The triplet pair spectrum and the 1 ms transient spectrum show good agreement, especially in the vicinity of the induced absorption feature at 510 nm. The presence of a small population of long-lived triplet excitations on the millisecond timescale could therefore also contribute to this signal, and would additionally serve to decrease the upper limit we established above (i.e., note the amplitude of the ground-state bleach associated with the scaled triplet excitation spectrum). We conclude that not only is the long-time signal marginal, the majority of the signal can be explained by sources other than those that represent alternative parallel decay pathways such as photodimerization.

We therefore consider the decay of the signal on the early timescale in the amorphous TIPS-Pn nanoparticles to arise primarily from a loss of stimulated emission, i.e., changes in the electronic structure of the exciton states as they convert from the parent singlet exciton to the triplet pair. Parallel decay pathways such as charge carrier formation and photodimerization would require some evidence for their presence, of which we have shown there is little to no evidence.<sup>13</sup> According to the arguments made above, we therefore estimate the triplet yield from singlet fission be ca. 194-200%, i.e., essentially quantitative. Such an estimate is reinforced through a simple kinetic analysis (**Section S14**), and is consistent with the statements made throughout the main text that the initial step of singlet fission is quantitative in both amorphous and crystalline material.

## Section S16: Five-component global and target analysis of transient visible absorption of amorphous TIPS-pentacene nanoparticles

The transient visible absorption of the amorphous TIPS-pentacene nanoparticles presented in the main text (**Fig. 2b**) were analyzed via a global and target analysis according to a five-component kinetic scheme (**Figure S14**).

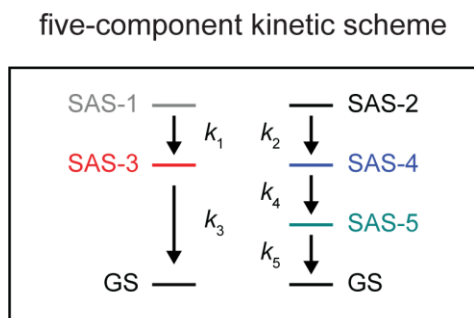


**Figure S14.** The five-component kinetic scheme used in the global and target analysis. The five-component scheme accounts for: (i) two distinct sets of parent singlet exciton and nascent triplet pair populations, i.e., SAS-1/SAS-3 and SAS-2/SAS-4, and (ii) long-lived, spatially separated triplet pairs, i.e., SAS-5.

Below we expound upon the main pieces of evidence supporting the use of a five-component kinetic scheme. These evidences include: (i) the presence of two distinct sets of parent singlet exciton and nascent triplet pair populations in the amorphous TIPS-Pn nanoparticles,<sup>14</sup> which establishes a four-component parallel scheme as that which is simplest and best describes the data, and (ii) the improved fitting of the data through the inclusion of an additional component in the model to account for triplet pair separation,<sup>2</sup> which establishes a five-component scheme (**Figure S14**) as that which is next simplest and best describes the data.

A four-component parallel kinetic scheme is that which is simplest and best describes the data. The main evidence supporting this argument is shown in **Figure S15**.

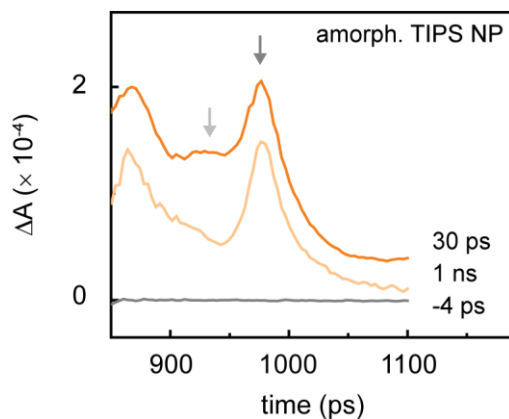


**Figure S15.** Transient near-infrared absorption spectra of amorphous TIPS-pentacene nanoparticles at time delays of -4 ps (grey), 30 ps (orange), and 1 ns (light orange). Grey and light grey arrows highlight two triplet induced absorption features present in the intermediate time delay spectrum (i.e., 30 ps) whose origin bands appear at ca. 980 and 930 nm, respectively.

**Figure S15** shows that two distinct triplet pair populations are evident in the transient near-infrared absorption spectrum of the amorphous TIPS-Pn nanoparticles measured immediately following the decay of parent singlet excitons. Specifically, two triplet induced absorption bands peaking at ca. 980 and 930 nm, attributable to two distinct triplet pair populations, are apparent at an intermediate time delay of ca. 30 ps. There is additional evidence indicating that the two triplet pair populations arise from two distinct parent singlet exciton populations. A complete proof of the model, including details pertaining to the identification and the nature of the different populations, are provided in a forthcoming contribution (ref. 14).

We previously showed that transient absorption spectroscopy can resolve two different triplet pair intermediates, and so directly time resolve triplet pair separation in singlet fission materials.<sup>2</sup> Accounting for the possibility that triplet pairs might spatially separate motivated us to include an additional component in the model (bringing the total number of components to five, see e.g. **Figure S14**). Including a fifth component in the model yielded a reduced rms value and improved residuals (**Figure S16**).

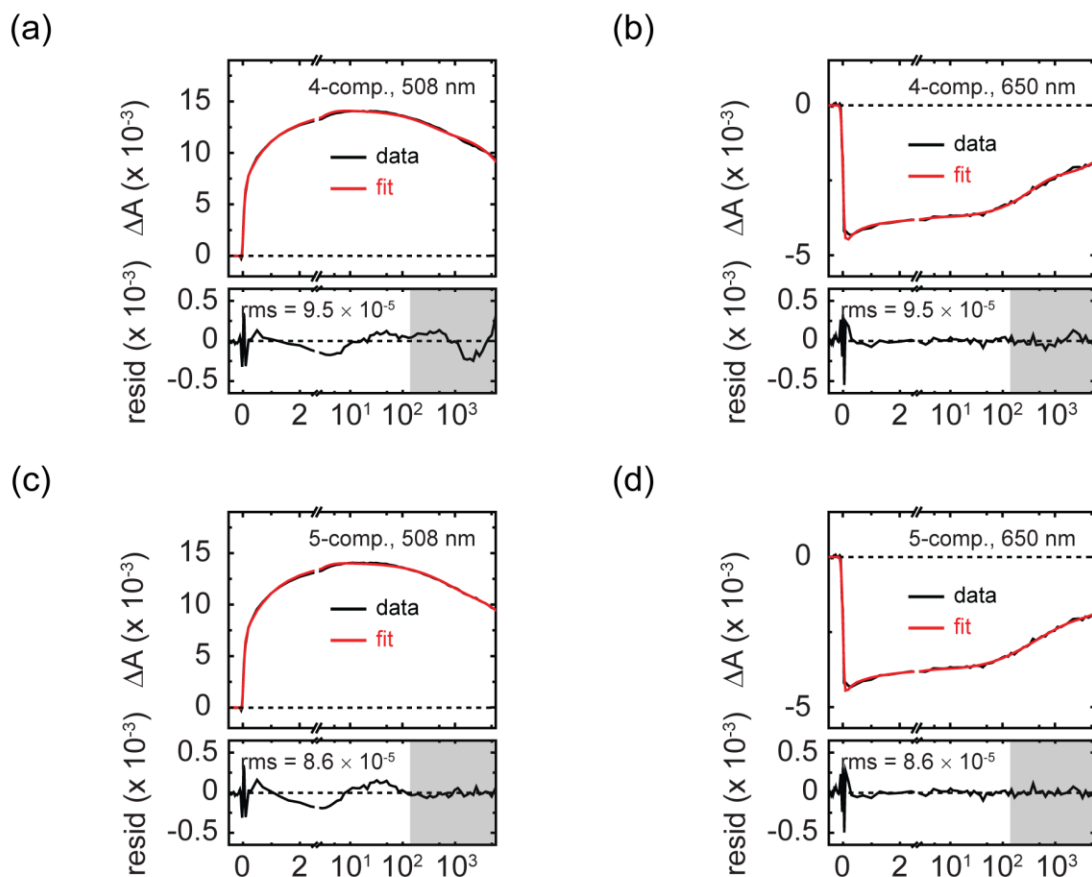


**Figure S16.** Selected transient kinetics traces in the vicinity of the origin band of the triplet photoinduced absorption and ground-state bleach feature at 508 and 650 nm, respectively, along with fits, rms values, and residuals from the global and target analysis. (a,b) Fits, rms values, and residuals associated with the four-component kinetic scheme. (c,d) Fits, rms values, and residuals associated with the five-component kinetic scheme. The grey blocks in each panel highlight regions where the residuals are improved by the inclusion of a fifth component.

Thus, the inclusion in the model of an additional, physically motivated component is justified on mathematical grounds. Below we show that the results of including this additional component in the model are consistent with physical expectations.

We next proceed to discuss the species-associated spectra and time constants derived by modelling the data according to the five-component kinetic scheme displayed in **Figure S14**. The species-associated spectra associated with two distinct sets of parent singlet exciton and triplet pair populations are presented in **Figure S17**.

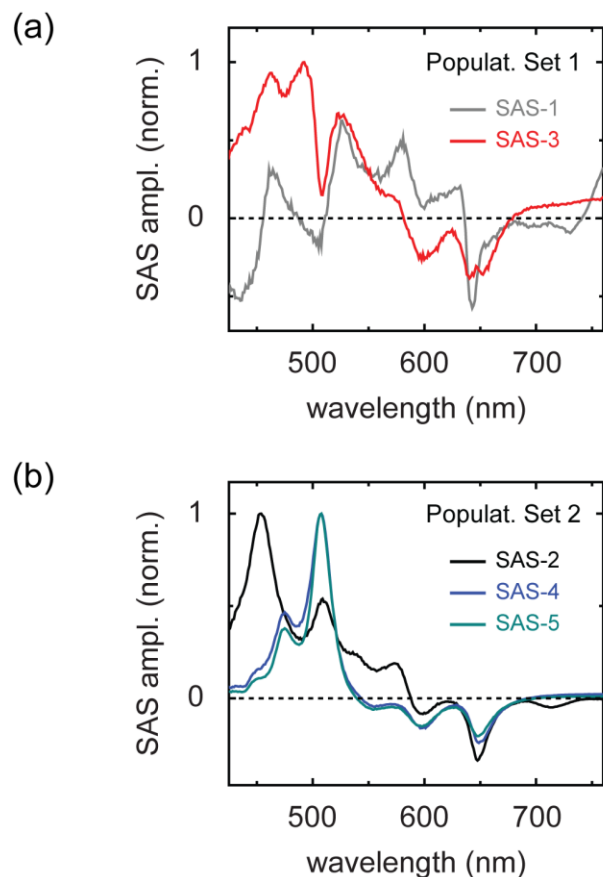


**Figure S17.** Species-associated spectra derived from a five-component global and target analysis of the transient absorption of the amorphous TIPS-pentacene nanoparticles. (a) Species-associated spectra SAS-1 (grey) and SAS-3 (red) attributable to a population set including short-lived parent singlet excitons and nascent triplet pairs. (b) Species-associated spectra SAS-2 (black), SAS-4 (blue), and SAS-5 (cyan) attributable to a population set including long-lived parent singlet excitons and nascent triplet pairs, the latter of which spatially separate.

The first and second components (i.e., SAS-1 and SAS-2) exhibit overall qualitatively similar spectral features, and are attributable to two different parent singlet exciton populations. **Table S1** shows that one of these populations is short-lived, while the other is comparatively longer-lived.

**Table S1.** Time Constants Determined by Modeling the Transient Absorption of the Amorphous TIPS-pentacene Nanoparticles According to a Five-Component Kinetic Scheme

$\tau_1$ (ps)	$\tau_2$ (ps)	$\tau_3$ (ps)	$\tau_4$ (ps)	$\tau_5$ (ps)
0.1	1.1	150	0.7	$\gg 8$

Specifically, SAS-1 has a lifetime of ca. 0.1 ps whereas SAS-2 has a lifetime of ca. 1.1 ps. The deviations of the SAS-1 spectrum that are especially apparent at wavelengths below ca. 520 nm likely originate from its short lifetime, which is of the order of the pump pulse duration (**Section**

**S25**) and therefore nonresonant response of the medium. The third and fourth components, i.e., SAS-3 and SAS-4, are associated with two different nascent triplet pair populations, the latter of which is able to spatially separate, i.e., SAS-5. Critically, the components accounting for the lifetime of the two triplet pair populations, i.e., SAS-3 and SAS-5, are found to be associated with drastically different time constants of ca. 150 ps and  $\gg 8$  ns, respectively. For the purpose of the present study, it is sufficient to acknowledge that the losses in the amorphous TIPS-Pn nanoparticles result from the presence of a triplet pair population that exhibits an exceedingly short excited-state lifetime.

We posited that while the short-lived triplet pair population may not be able spatially separate due of its short lifetime, the long-lived triplet pair population may be capable of triplet pair separation. An additional component, SAS-4, accounts for triplet pair separation. The timescale of triplet pair separation in the amorphous nanoparticles is found to be ca. 0.7 ps. Further supporting the inclusion of this additional component in the model, the species-associated spectra derived from the global target analysis representative of the two triplet pair intermediates, labelled as SAS-4 and SAS-5 in **Figures S17b**, exhibit expected variations.<sup>2,15</sup> Namely, we observe additional signal amplitude in the nascent triplet pair spectrum (i.e., SAS-4) in regions overlapping the parent singlet photoinduced absorption, specifically at wavelengths in the vicinity of ca. 460 and 560 nm where these features are comparatively strong.

The time constant associated with triplet pair separation in the amorphous TIPS-Pn nanoparticles was found to be of the order of ca. 1 ns. It is informative to compare the time constant measured for triplet pair separation in the amorphous TIPS-Pn nanoparticles with that measured for triplet pair separation in the crystalline TIPS-Pn nanoparticles (**Section S10**). We note that a triplet pair separation time constant of the order of a few ps has been measured for a series of crystalline pentacene derivative solids (see e.g. refs. 1 – 3). We immediately see that the time constant associated with triplet pair separation in the amorphous TIPS-Pn nanoparticles is three orders-of-magnitude larger than that observed in crystalline material. Our derivation of picosecond timescale triplet pair separation in crystalline TIPS-Pn nanoparticles (**Section S10**) and nanosecond timescale triplet pair separation in amorphous TIPS-Pn nanoparticles (**Section S16**) further verifies our assignment of the solid-state order of the nanoparticles. Specifically, the elementary step associated with triplet pair separation, i.e., triplet transfer, is expected to depend sensitively on molecular-level packing. That is, the timescale of triplet transfer is known to vary exponentially with distance.<sup>16</sup> Because the average intermolecular distance in amorphous material can be expected to be larger than that in crystalline material (at least as a first approximation), we can expect the timescale of triplet transfer to be longer in amorphous material. The time constant associated with triplet transfer in amorphous solids is, in fact, generally expected to be appreciably slower,<sup>17</sup> and indirect evidence of this is manifested in amorphous and crystalline TIPS-Pn films where much lower triplet diffusivities were measured for the former.<sup>1</sup> We thus conclude this section highlighting additional evidence confirming our assignment of the solid-state order of the amorphous and crystalline pentacene derivative nanoparticles.

## Section S17: Identical losses are observed in amorphous TIPS-pentacene films

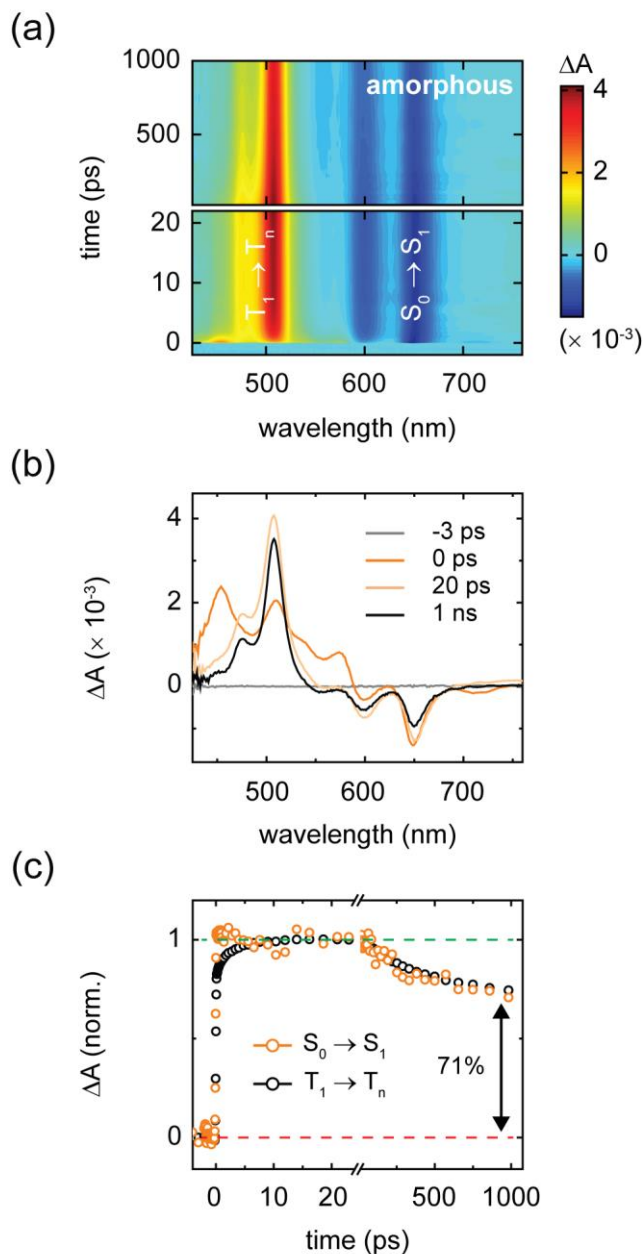


**Figure S18.** Transient visible absorption of amorphous films of TIPS-pentacene. (a) Surface plot of transient visible absorption of amorphous TIPS-pentacene films. The experiment was performed with an incident pump fluence of  $40 \mu\text{J}/\text{cm}^2$ . The scale bar is indicated. (b) Selected transient spectra for amorphous TIPS-pentacene films. Spectra time delays are indicated in the legend. (c) Selected transient kinetics for amorphous TIPS-Pn films. These kinetics were taken as the average over the spectral range 490 to 560 nm and 630 to 690 nm, respectively, and have been normalized over the time range from 5 to 20 ps.

## **Section S18: Singlet and triplet excitation migration in amorphous TIPS-pentacene nanoparticles are not susceptible to bimolecular annihilation**

*Singlet excitation migration in amorphous TIPS-pentacene nanoparticles is not susceptible to bimolecular annihilation*

The manner in which we chose to probe the migration of singlet excitation energy from amorphous to crystalline domains in the neat and mixed-phase nanoparticles was through the decay kinetics of the parent singlet photoinduced absorption transition appearing in the near-infrared. This transition is especially advantageous because its origin band, which peaks at ca. 1400 nm, does not overlap with the near-infrared triplet photoinduced absorption features associated with either amorphous or crystalline material (**Fig. 3b, inset**). In the main text, we report transient absorption measurements performed at an incident pump fluence of 260  $\mu\text{J}/\text{cm}^2$ . In order to ensure that our results are not complicated by bimolecular annihilation at this pump fluence, which could lead to an erroneous interpretation, we evaluated the extent to which the excited-state dynamics in the amorphous TIPS-Pn nanoparticles were influenced by incident pump fluence.

As we show in the main text and above (i.e., **Figs. 2b,d,f** and **Sections S14-S17**), singlet fission is the primary decay pathway in amorphous solids of TIPS-Pn. Thus, we can measure the signal associated with the triplet pair population to evaluate whether or not any singlet-singlet annihilation occurs prior to the complete decay of parent singlet excitons. This signal should track linearly with incident pump fluence in the absence of singlet-singlet annihilation; any amount of singlet-singlet annihilation preceding triplet pair formation, which can especially become apparent at excessive fluences, would serve to reduce the overall yield of triplet pairs and cause the signal to deviate from linearity. We therefore evaluated the amorphous TIPS-Pn nanoparticles for singlet-singlet annihilation by measuring the linearity of the signal associated with the triplet pair population at a time delay of ca. 50 ps, i.e., a timescale well beyond that associated with the complete decay of parent singlet excitons and formation of triplet pairs (**Figure S19a**).

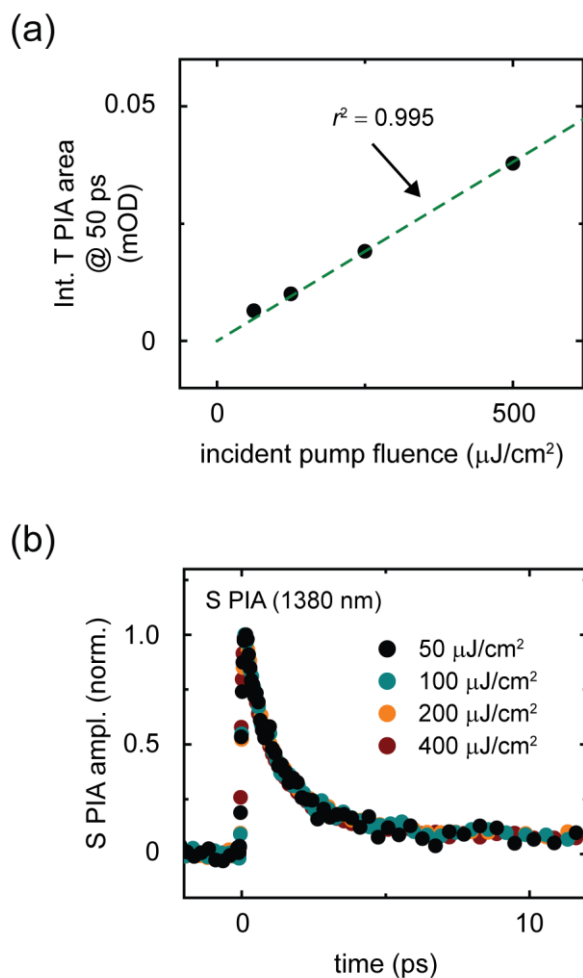


**Figure S19.** Transient absorption measurements of amorphous TIPS-pentacene nanoparticles evaluating the influence of fluence on the propensity for singlet-singlet annihilation. (a) Integrated area of the triplet photoinduced absorption band in the near-infrared spectral region (i.e., ca. 850-1050 nm) at a time delay of ca. 50 ps plotted as a function of incident pump fluence. Overlaying the data is a linear fit (green dashed line) with  $r^2 = 0.995$ . (b) Amplitude near the peak of the origin band of singlet photoinduced absorption in the near-infrared spectral region (i.e., ca. 1380 nm) plotted at several incident pump fluences as a function of time delay. The data were normalized to the signal amplitude at a time delay in the vicinity of the time origin of the measurement.

The results show that the triplet pair signal measured at a time delay of 50 ps is linearly correlated with incident pump fluence (**Figure S19a**), evidencing the absence of any appreciable singlet-singlet annihilation in the amorphous nanoparticles.

We additionally confirmed that the decay kinetics associated with the near-infrared parent singlet photoinduced absorption feature were independent of incident pump fluence (**Figure S19b**). In **Figure S19b**, we show that the decay kinetics associated with this spectral feature are independent of incident pump fluences up to values as high as ca. 400  $\mu\text{J}/\text{cm}^2$ . We therefore conclude that singlet excitation energy in amorphous TIPS-Pn nanoparticles is not susceptible to

bimolecular annihilation, and that the decay kinetics are not influenced by incident pump fluence. Taking together, and also recalling our observation above that singlet excitation energy is not susceptible to bimolecular annihilation in the crystalline TIPS-Pn nanoparticles (**Section S12**), we conclude that bimolecular annihilation will have no influence on our approach comparing changes in the rate of decay of the parent singlet exciton population in the neat and mixed-phase nanoparticles as a way to elucidate whether or not singlet excitation energy migrates between amorphous and crystalline domains.

*Triplet excitation migration in amorphous TIPS-pentacene nanoparticles is not susceptible to bimolecular annihilation*

In the main text, we also evaluated whether or not triplet excitation energy migrates between amorphous and crystalline domains. To do this, we selectively excited amorphous chromophores and observed at long time delays (i.e., ca. 1 ns) whether or not the resultant triplet photoinduced absorption bands were representative of triplets located in amorphous or crystalline material. To effectively make this evaluation, we must ensure that triplet excitation energy is not annihilating with amorphous domains.

As such, we next studied the fluence-dependence of the triplet excitation population in the amorphous TIPS-Pn nanoparticles (**Figure S20**).

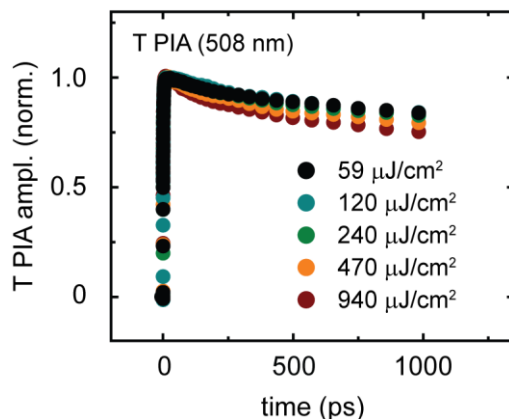


**Figure S20.** Amplitude near the peak of the origin band of the triplet photoinduced absorption appearing in the near-infrared spectral region (i.e., ca. 508 nm) plotted at several incident pump fluences as a function of time delay. The data were normalized to the signal amplitude at a time delay of ca. 20 ps.

In **Figure S19a**, we showed that the triplet photoinduced absorption signal observed at 50 ps was linearly correlated with incident pump fluence which indicates that the triplet excitation population does not exhibit any bimolecular annihilation out to this timescale. To probe the fluence dependence of this population at longer time delays, i.e., out to a timescale of 1 ns, we probed the strong photoinduced absorption band associated with TIPS-Pn triplet excitations that appears in the visible spectral region (see e.g. **Fig. 2d** and **Section S13**). **Figure S20** shows the measured fluence dependence of this triplet photoinduced band out to a timescale of 1 ns. We find that while

the kinetics of the triplet photoinduced absorption band do show some slight changes at incident pump fluences of  $470 \mu\text{J}/\text{cm}^2$  and higher, the decay kinetics associated with this feature did not show appreciable deviation up to incident pump fluences as high as  $240 \mu\text{J}/\text{cm}^2$ , i.e., similar to that used for the measurements reported in the main text.

We thus conclude there is no triplet-triplet annihilation within amorphous domains on the timescale of the measurement at the incident pump fluences used for the measurements reported in this work, and therefore that it is feasible to evaluate long-time transient absorption spectra measured in the mixed-phase nanoparticles to elucidate whether or not triplet excitation energy migrates from amorphous to crystalline domains on a few nanosecond timescale.

## Section S19: Parameters varied to prepare samples of mixed morphologies

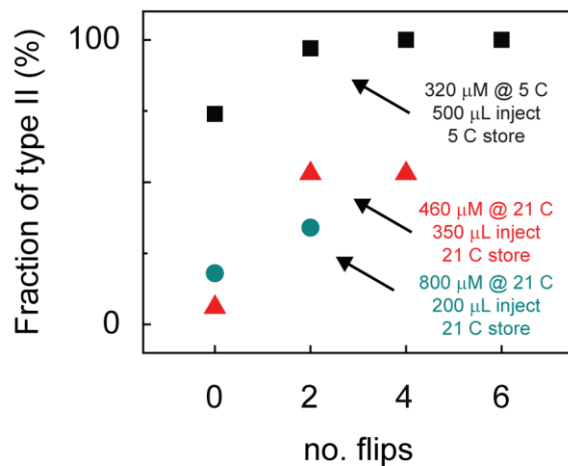


**Figure S21.** Fraction of crystalline material as a function of the number of syringe flips prior to injection of the TIPS-Pn / THF solution. Several additional parameters of the sample preparation, including the injection solution concentration and volume and the storage temperature, were also varied in order to finely control solid-state order and morphology of the nanoparticles. The specific concentrations, volumes, and temperatures varied appear next to the corresponding data points in the figure.

## **Section S20: Assignment to mixed-phase nanoparticles over a mixture of pure-phase amorphous and crystalline nanoparticles**

It is described why it is highly unlikely that the mixed-phase nanoparticle suspensions constitute a simple mixture of pure-phase (or neat) amorphous and crystalline nanoparticles. Rather, it is argued that the nanoparticle suspensions more likely consist of a distribution of mixed-phase nanoparticles.

The majority of the argument rests on a fundamental understanding of the way in which the nanoparticles are prepared. The TIPS-Pn nanoparticles in the present work are prepared by rapid precipitation—a large amount of TIPS-Pn is dissolved in tetrahydrofuran (THF), a “good” solvent and this concentrated TIPS-Pn solution is then rapidly injected into water, a “bad” solvent. Nanoparticles form at nucleation sites primarily as a result of the supersaturation conditions imposed by the rapidly formed binary solvent mixture along with the immiscibility of TIPS-Pn in water.<sup>18</sup> Assuming that both TIPS-Pn and additive are homogeneously dispersed throughout the THF solution prior to its injection into water, it is reasonable to assume that both TIPS-Pn and additive are also homogeneously dispersed at the nucleation sites where the nanoparticles form. Additionally, as a result of the additive’s immiscibility in water, it is expected that any additive in the vicinity of the TIPS-Pn will co-precipitate along with it. Therefore, because both TIPS-Pn and additive are expected to be homogeneously dispersed at the nanoparticle nucleation sites and because they are expected to co-precipitate together at these nucleation sites, we consider the additive to be homogeneously mixed in the nanoparticles.

It is possible that a disproportionate amount of additive is introduced into one nanoparticle versus the next. Specifically, it might be possible that one nanoparticle does not incorporate any additive, another nanoparticle incorporates some additive, and a third nanoparticle incorporates a substantial amount of additive. Therefore, we consider the nanoparticles studied in the present work to constitute a distribution of morphologies potentially spanning neat amorphous to mixed-phase amorphous/crystalline to neat crystalline. A quantitative evaluation of this distribution is beyond the scope of the present work.

## Section S21: Extinction spectra of crystalline and amorphous TIPS-pentacene nanoparticles

The aqueous colloidal suspensions of TIPS-Pn nanoparticles provide a convenient means in which to measure the extinction spectra of amorphous and crystalline material and estimate the amount of each in the mixed-phase TIPS-Pn nanoparticles. We found that the extinction at the peak of the lowest-energy singlet exciton transition decreased when the chromophores converted from amorphous to crystalline, consistent with strong excitonic coupling reported previously in nanoparticles of several other pentacene derivatives.<sup>3</sup> The value of ca.  $7,000 \text{ M}^{-1} \text{ cm}^{-1}$  for the extinction at the peak of the lowest-energy singlet transition in the crystalline TIPS-Pn nanoparticles compares very well with the extinction reported for chromophores in crystalline thin films of TIPS-Pn.<sup>19</sup>

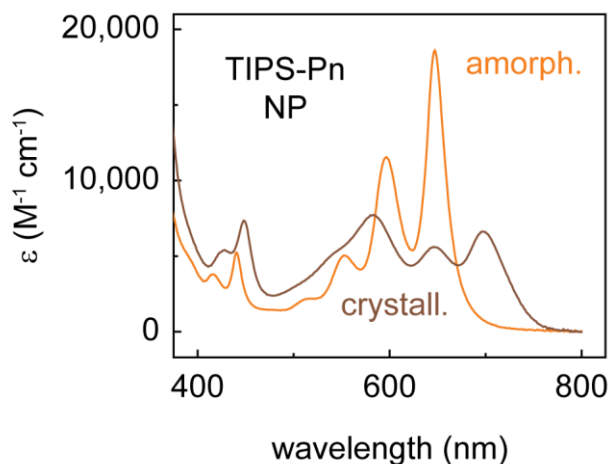


**Figure S22.** Extinction spectra of aqueous colloidal suspensions of amorphous and crystalline TIPS-Pn nanoparticles.

## **Section S22: Migration of excitation energy between nanoparticles is not possible on the timescale of the femtosecond transient absorption measurements**

In this section, we show that the migration of excitation energy between nanoparticles is not possible on the timescale of the femtosecond transient absorption measurements.

We first consider the diffusivity of the nanoparticles within the nanoparticle suspension. The diffusivity of the nanoparticles can be described by the Stokes-Einstein equation:

$$D = (k_B T) / (6 \pi \eta r)$$

where  $k_B$  is Boltzmann's constant,  $T$  is temperature,  $\eta$  is the dynamic viscosity, and  $r$  is the radius of the spherical nanoparticles. The dynamic viscosity of water at a temperature of 21 °C corresponds to  $0.982 \times 10^{-3}$  N-s/m<sup>2</sup>.<sup>20</sup> The radius of the TIPS-Pn nanoparticles has been measured via dynamic light scattering to be ca. 35 nm.<sup>3</sup> Plugging these values into the Stokes-Einstein equation above gives a diffusivity of  $6.26 \times 10^{-8}$  cm<sup>2</sup>/s.

The distance over which the nanoparticles can diffuse over the course of the timescale of the femtosecond transient absorption measurement can be estimated by considering the relationship between diffusivity, diffusion length, and lifetime:

$$L_D = \sqrt{(D \tau)}$$

where  $L_D$  is diffusion length and  $\tau$  is lifetime. We consider here the timescale of ca. 8 ns to represent a proxy lifetime, i.e., the maximum duration of the femtosecond transient absorption measurement. Plugging these values into the equation above yields a diffusion length of ca.  $2.34 \times 10^{-8}$  cm. Thus, the nanoparticles traverse a distance of ca. 0.2 nm over the course of the transient absorption measurement.

We next consider the mean distance between nanoparticles. This can be estimated by first considering the number of molecules comprising a single nanoparticle, and subsequently by considering the nanoparticulate concentration derived from the molar concentration.

The number of molecules comprising a single nanoparticle can be determined using an expression for the volume of the nanoparticle along with the mass density and molar mass of the molecular constituents making of the nanoparticle. In this case, we assume the nanoparticles have a spherical shape, with prior imaging results on pentacene derivative nanoparticles in support of this interpretation.<sup>3</sup> Thus, the volume of the nanoparticle can be calculated as:

$$V_{NP} = (4/3) \pi r^3$$

Taking the radius of 35 nm noted above, gives a nanoparticle volume of  $1.8 \times 10^{-16}$  cm<sup>3</sup>. We can now determine the mass of the nanoparticle, given the density of the nanoparticle, which for the purpose of the present estimation, we assume is 1.1 g/cm<sup>3</sup> or that of crystalline TIPS-Pn.<sup>21,22</sup> With these values for volume and density, we determine a nanoparticle mass of  $2.0 \times 10^{-16}$  g. Lastly, we

can take the mass of the nanoparticle along with the molar mass of TIPS-Pn (639 g/mol) and Avogadro's number to determine that there are ca. 190,000 molecules per nanoparticle.

The mean distance between nanoparticles is then determined by considering the concentration of the nanoparticles in the measurement. The concentration of the nanoparticles can be determined using Beer's law:

$$A = \epsilon b c$$

where  $A$  is the absorbance,  $\epsilon$  is the molar extinction of the nanoparticles,  $b$  is the pathlength, and  $c$  is the concentration. The absorbance of the sample for the present measurement was ca. 0.32. We can estimate the molar extinction of the nanoparticles as the extinction of a single chromophore times the number of molecules (or chromophores) per nanoparticle. We measured the extinction for a single chromophore in the amorphous nanoparticles to be ca.  $24,000 \text{ M}^{-1} \text{ cm}^{-1}$  at the peak maximum of the 0-0 vibronic band of the lowest-energy singlet transition (i.e., ca. 646 nm). With the number of molecules per nanoparticle determined above, this gives a molar extinction of  $4.5 \times 10^9 \text{ M}^{-1} \text{ cm}^{-1}$  for the nanoparticles. The molar concentration of the nanoparticles can now be determined for a path length of 0.2 cm and absorbance of 0.32. The molar concentration determined in this manner is  $3.6 \times 10^{-10} \text{ M}$ . The molar concentration can be converted to nanoparticle concentration using Avogadro's number and conversion of units to give  $2.2 \times 10^{11}$  nanoparticles /  $\text{cm}^3$ . Lastly, we can estimate the mean distance between nanoparticles by taking the third root of the inverse of the nanoparticle concentration. This gives a value of  $1.7 \times 10^{-4} \text{ cm}$  or 1,700 nm.

Thus, while the nanoparticles are separated by a mean distance of ca. 1,700 nm as a consequence of their density in solution, the nanoparticles only traverse a distance of 0.2 nm over the course of the timescale of the time-resolved measurement. On the basis of the large difference in the relative magnitude of these distances, we rule out the possibility of migration of excitation energy between nanoparticles on the timescale of the femtosecond transient absorption measurements.

### Section S23: Films with mixed morphology also do not show evidence for parent singlet exciton migration between amorphous and crystalline domains

We additionally explored the possibility that parent singlet excitons might migrate between amorphous and crystalline domains in films, but not in the nanoparticles. Neat amorphous and crystalline films and a mixed morphology film were prepared (**Fig. S23a**) in a manner described previously.<sup>1</sup> Using a two-phase model to describe the absorption spectra of the mixed morphology film yields a composition of ca. 40% amorphous and 60% crystalline material. With such high loading of crystalline material, this result suggests the probability for singlet exciton migration between amorphous and crystalline domains in the mixed morphology film to be quite high.

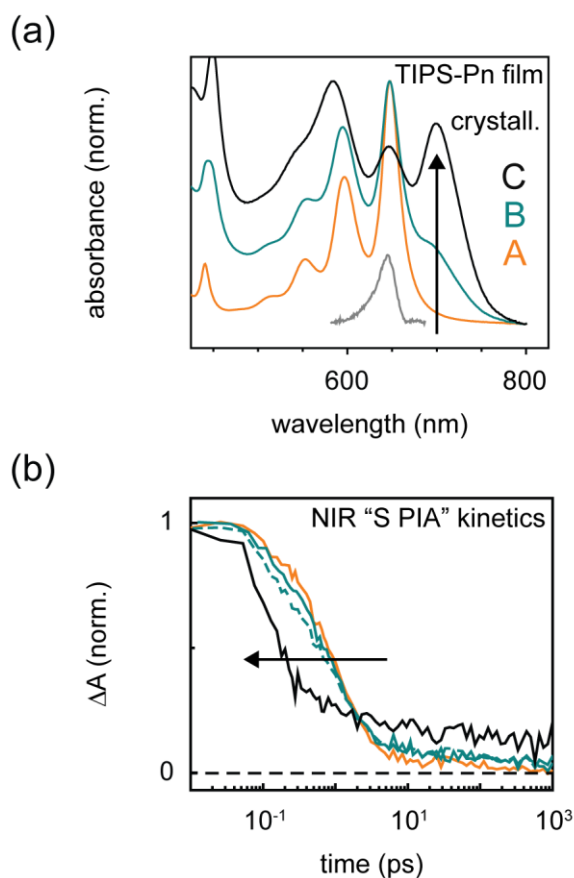


**Figure S23.** Amorphous, mixed morphology, and crystalline TIPS-pentacene films. (a) Steady-state absorption spectra of the neat amorphous and crystalline TIPS-pentacene films and mixed morphology TIPS-pentacene film. The spectra were normalized to the most intense feature appearing in the vicinity of the lowest-energy singlet transition. The spectrum of the pump used in the transient absorption experiments to selectively excite chromophores in the amorphous regions is shown in grey and is scaled for clarity. (b) Kinetics of the parent singlet near-infrared photoinduced absorption appearing in the amorphous, mixed morphology, and crystalline TIPS-pentacene films. The measurements were performed at a pump wavelength of 645 nm and incident pump fluence of ca.  $80 \mu\text{J}/\text{cm}^2$ . The data were normalized to the maximum amplitude occurring near the time origin of the measurement. The dashed line is the decay of the mixed morphology

film predicted by taking an appropriately weighted sum of the neat amorphous and crystalline film decays.

To probe whether or not parent singlet excitons migrate between amorphous and crystalline domains in the mixed morphology film, we monitored the decay of parent singlet excitons as in the main text through a feature appearing in the near-infrared at ca. 1400 nm (**Fig. S23b**). As we find in the main text (**Fig. 3b**) in the mixed morphology nanoparticles, the decay of the parent singlet exciton feature does not accelerate substantially relative to the predicted decay taking an appropriately weighted sum of the neat amorphous and crystalline film decays. This result indicates that even in the mixed morphology film with substantial loading of crystalline material, singlet fission within an amorphous domain kinetically outcompetes the migration of parent singlet excitons between amorphous and crystalline domains.

## Section S24: Transient near-infrared absorption of neat and mixed-phase TIPS-pentacene nanoparticles

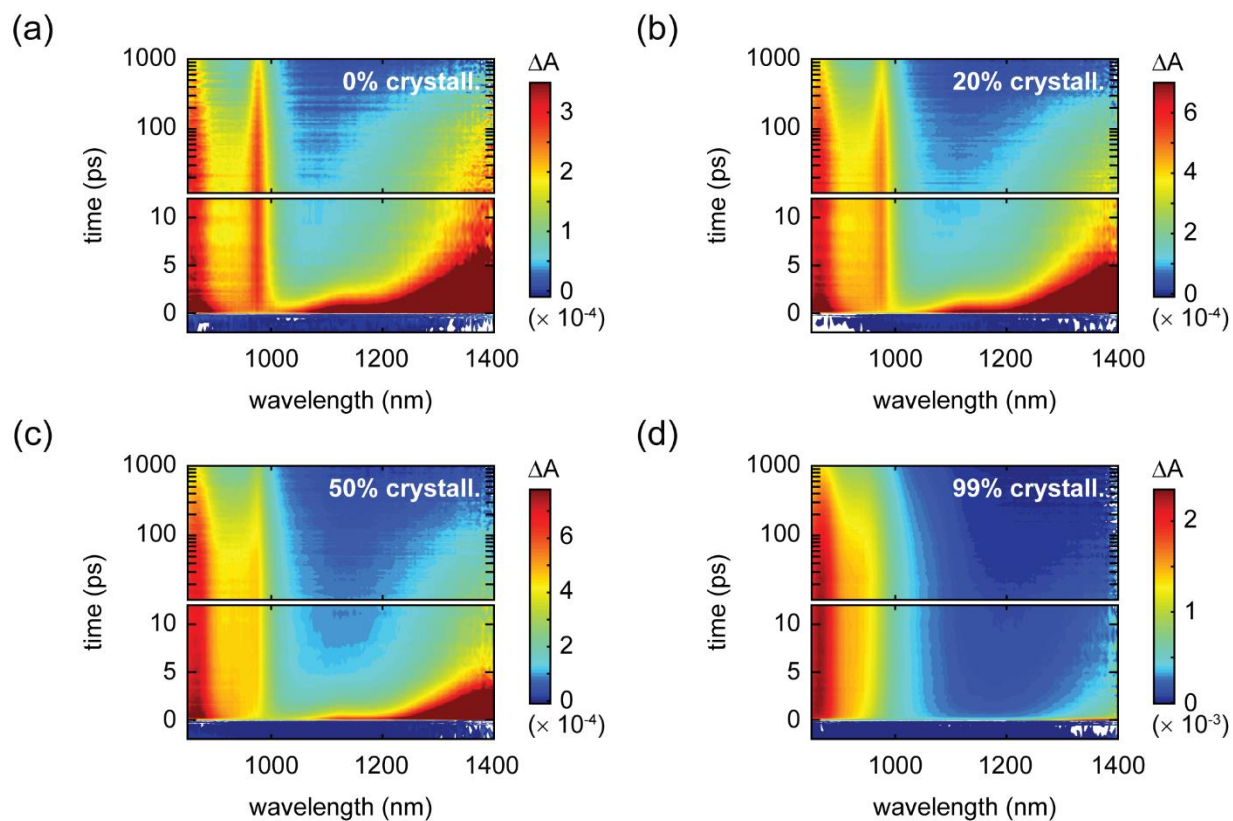


**Figure S24.** Transient near-infrared absorption of neat and mixed-phase TIPS-pentacene nanoparticles. The measurements were performed on (a) 0%, (b) 20%, (c) 50%, and (d) 99% crystalline nanoparticles with a pump wavelength of 645 nm and at an incident pump fluence of ca.  $260 \mu\text{J}/\text{cm}^2$ . The parent singlet photoinduced absorption peaking at ca. 1400 nm appears off-scale in order to highlight the time evolution of the comparatively weaker triplet photoinduced absorptions appearing at shorter wavelengths.

## Section S25: Pump pulse autocorrelation

An autocorrelation was performed to estimate the pump pulse duration at the sample position. The beam was redirected following several reflections after the OPA to the autocorrelator. A comparable amount of glass (ca. 5 mm) was placed in the beam path prior to the autocorrelator to simulate the experimental conditions, specifically the transmissive optics prior to the sample position in the transient absorption spectrometer. The autocorrelation resulted in a FWHM of ca.  $110 \pm 5$  fs at a wavelength of 710 nm.

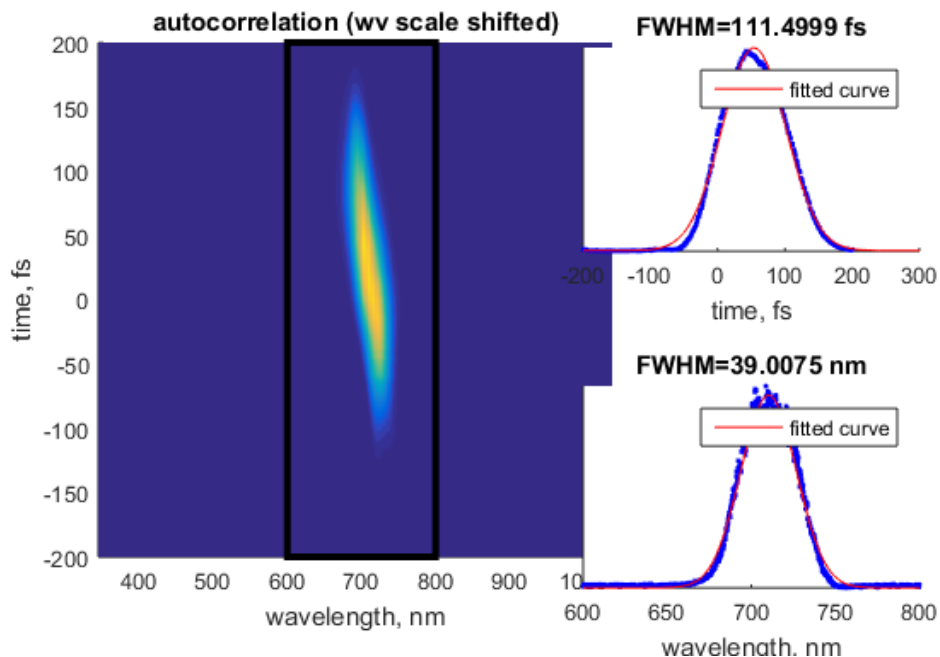


**Figure S25.** Representative autocorrelation of 710 nm pump. Three independent measurements resulted in a FWHM of  $110 \pm 5$  fs.

## **Section S26: Supplementary methods**

### **Dynamic light scattering**

Dynamic light scattering measurements were performed on a Malvern Instruments Zetasizer Nano ZS instrument equipped with a HeNe laser ( $\lambda = 633 \text{ nm}$ ).

### **Spectroelectrochemistry**

The spectroelectrochemistry setup consists of a Bioanalytical Systems Epsilon potentiostat coupled to a Varian 5000 UV-Vis-NIR spectrophotometer. The TIPS-Pn cation absorption spectrum was measured in dry, deoxygenated dichloromethane solution at room temperature using 0.1 M tetrabutylammonium hexafluorophosphate as electrolyte. A platinum mesh working electrode, platinum wire counter electrode, and a silver reference electrode were used. A constant cell potential of +1000 mV was used to generate the  $[\text{TIPS-Pn}]^+$  species.

The TIPS-Pn monoanion absorption spectrum was recorded following chemical reduction of TIPS-Pn using sodium metal in rigorously dried, deoxygenated THF at room temperature. A solution of the anionic species was transferred into a sealable quartz cuvette, and absorption spectra recorded every 30 minutes (over a period of ~15 hours). Generation of monoanionic TIPS-Pn was confirmed by evolution of the spectral features over time, clearly showing direct conversion of neutral  $[\text{TIPS-Pn}]$  to  $[\text{TIPS-Pn}]^-$ .

## **Section S27: References**

- 1 C. Grieco, G. S. Doucette, R. D. Pensack, M. M. Payne, A. Rimshaw, G. D. Scholes, J. E. Anthony and J. B. Asbury, *J. Am. Chem. Soc.*, 2016, **138**, 16069–16080.
- 2 R. D. Pensack, E. E. Ostroumov, A. J. Tilley, S. Mazza, C. Grieco, K. J. Thorley, J. B. Asbury, D. S. Seferos, J. E. Anthony and G. D. Scholes, *J. Phys. Chem. Lett.*, 2016, 2370–2375.
- 3 R. D. Pensack, A. J. Tilley, S. R. Parkin, T. S. Lee, M. M. Payne, D. Gao, A. A. Jahnke, D. G. Oblinsky, P.-F. Li, J. E. Anthony, D. S. Seferos and G. D. Scholes, *J. Am. Chem. Soc.*, 2015, **137**, 6790–6803.
- 4 Y. Liu, K. Kathan, W. Saad and R. K. Prud'homme, *Phys. Rev. Lett.*, 2007, **98**, 36102.
- 5 N. J. Turro, J. C. Scaiano and V. Ramamurthy, *Modern Molecular Photochemistry of Organic Molecules*, University Science Books, Sausalito, CA, 2010.
- 6 J. J. Burdett, A. M. Müller, D. Gosztola and C. J. Bardeen, *J. Chem. Phys.*, 2010, **133**, 144506.
- 7 A. D. Platt, J. Day, S. Subramanian, J. E. Anthony and O. Ostroverkhova, *J. Phys. Chem. C*, 2009, **113**, 14006–14014.
- 8 S. R. Yost, J. Lee, M. W. B. Wilson, T. Wu, D. P. McMahon, R. R. Parkhurst, N. J. Thompson, D. N. Congreve, A. Rao, K. Johnson, M. Y. Sfeir, M. G. Bawendi, T. M. Swager, R. H. Friend, M. A. Baldo and T. Van Voorhis, *Nat. Chem.*, 2014, **6**, 492–497.
- 9 A. J. Musser, M. Liebel, C. Schnedermann, T. Wende, T. B. Kehoe, A. Rao and P. Kukura, *Nat. Phys.*, 2015, **11**, 352–357.
- 10 M. Pope and C. E. Swenberg, *Electronic processes in organic crystals and polymers*, Oxford University Press, New York, 2nd ed., 1999.
- 11 B. A. Gregg, *J. Phys. Chem. B*, 2004, **108**, 17285–17289.
- 12 We note that the pump spectrum reported in **Figure S13c** is not that actually used for the measurements (we did not acquire the spectrum of the pump pulse used for the experiments performed on that day). For the plot, we set the spectrometer to a pump wavelength similar to that used in the measurements for the current work.
- 13 It is worthwhile to note that while we have ruled out charge carrier formation and photodimerization as major parallel decay pathways, we cannot rule them out completely (i.e., as having a minor contribution). Taking the latter as an example, the amorphous TIPS-Pn nanoparticles have a propensity to photochemically degrade over the course of time (i.e., days to months) with light exposure, and so there must be some probability of forming photodimers following light excitation. However, this probability is apparently so low as to not be readily detectable in transient absorption measurements, likely as a result of the limits of sensitivity of the method.
- 14 R. D. Pensack, *et al.*, 2017, in preparation.
- 15 H. L. Stern, A. J. Musser, S. Gelinas, P. Parkinson, L. M. Herz, M. J. Bruzek, J. Anthony, R. H. Friend and B. J. Walker, *Proc. Natl. Acad. Sci.*, 2015, **112**, 7656–7661.
- 16 G. L. Closs, P. Piotrowiak, J. M. MacInnis and G. R. Fleming, *J. Am. Chem. Soc.*, 1988, **110**, 2652–2653.
- 17 A. Köhler and H. Bässler, *Electronic Processes in Organic Semiconductors: An Introduction*, Wiley-VCH, Weinheim, 2015.
- 18 W. S. Saad and R. K. Prud'homme, *Nano Today*, 2016, **11**, 212–227.
- 19 C. Ramanan, A. L. Smeigh, J. E. Anthony, T. J. Marks and M. R. Wasielewski, *J. Am. Chem. Soc.*, 2012, **134**, 386–397.

- 20 J. C. Crittenden, R. R. Trussell, D. W. Hand, K. J. Howe and G. Tchobanoglous, *MWH's Water Treatment: Principles and Design*, Wiley, Hoboken, NJ, 3rd edn., 2012.
- 21 J. E. Anthony, J. S. Brooks, D. L. Eaton and S. R. Parkin, *J. Am. Chem. Soc.*, 2001, **123**, 9482–9483.
- 22 It should be noted that taking the density of crystalline material as that for amorphous material obviously is a rather extreme assumption, although the density of crystalline material can also be taken to represent an upper bound for the density of amorphous material. In other words, the density of amorphous material is expected to be slightly less than that of crystalline material. This discrepancy does not significantly impact the conclusions of the present estimation.